Bull. Mater. Sci., Vol. 34, No. 2, April 2011, pp. 207–216. © Indian Academy of Sciences.

Metal-coated magnetic nanoparticles for surface enhanced Raman scattering studies

G V PAVAN KUMAR, N RANGARAJAN, B SONIA, P DEEPIKA, NASHIOUR ROHMAN and CHANDRABHAS NARAYANA*

Chemistry and Physics of Materials Unit, Jawaharlal Nehru Centre for Advanced Scientific Research, Bangalore 560 064, India

MS received 23 August 2008

Abstract. **We report the optimization and usage of surfactantless, water dispersible Ag and Au-coated γ–Fe_2O_3 nanoparticles for applications in surface-enhanced Raman scattering (SERS). These nanoparticles, with plasmonic as well as super paramagnetic properties exhibit Raman enhancement factors of the order of 10^6 (10^5) for Ag (Au) coating, which are on par with the conventional Ag and Au nanoparticles. Raman markers like 2-naphthalenethiol, rhodamine-B and rhodamine-6G have been adsorbed to these nanoparticles and tested for nonresonant SERS at low concentrations. Further, to confirm the robustness of Ag-coated nanoparticles, we have performed temperature-dependent SERS in the temperature range of 77–473 K. The adsorbed molecules exhibit stable SERS spectra except at temperatures >323 K, where the thermal desorption of test molecule (naphthalenethiol) were evident. The magnetic properties of these nanoparticles combined with SERS provide a wide range of applications.**

Keywords. **Surface-enhanced Raman scattering; magnetic nanoparticles; core-shell nanostructure; bio-diagnosis.**

1. Introduction

In recent years, plasmonic nanostructures exhibiting novel optical properties have attracted enormous attention (Barnes *et al* 2003; Jin *et al* 2003; Genet and Ebbesen 2007; Vlaminck *et al* 2007; Wurtz *et al* 2007). The optical properties of plasmonic nanostructures are varied and can be tuned by using different metals in various geometrical configurations at the nano-scale (Thomas *et al* 2004; Shibu *et al* 2006; Pramod *et al* 2007). New developments in plasmonic nanostructures have a great impact on various analytical techniques, like surface-enhanced Raman scattering (SERS) (Baker and Moore 2005; Dieringer *et al* 2006), tip-enhanced Raman scattering (Zhang *et al* 2007a), surface plasmon resonance (Hutter and Fendler 2004), metal-enhanced fluorescence (Aslan *et al* 2007; Previte *et al* 2007; Zhang *et al* 2007b); in which metallic nano-surfaces play an important role. Especially, in SERS, the nature of the metal, surface morphology and roughness, geometrical configuration, etc has an important consequence on electromagnetic and chemical enhancement mechanisms, the two basic principles underlying the phenomenon (Moskovits 1982; Campion and Kambhampati 1998; Kneipp *et al* 2006).

Two of the most extensively used metallic nanoparticles for SERS applications are silver- and gold-based (Kneipp *et al* 1999). Another interesting nano-architecture is the core-shell configuration, where either a dielectric or a metallic core (usually spherical) can be coated with metallic shells. There are various interesting properties of core-shell nanoparticles, which are not observed in conventional metallic nanoparticles, like tunable surface plasmon resonance (Freeman *et al* 1996; Kumar *et al* 2007) and formation of SERS hot spots on a single nanoparticle (Kumar *et al* 2007). Another variation on the same stream of thought is the magnetic core-metallic shell nanoparticles, which exhibits both magnetic and plasmonic properties (Xu *et al* 2007). This configuration has opened new avenues in bio-sensing, where two different physical properties of same nanoparticles can be harnessed for detection. Previously, different synthetic routes have been devised to prepare the metal-coated magnetic nanoparticles for specific applications (Mandal *et al* 2005; Kouassi and Irudayaraj 2006). Recently, gold-coated magnetic nanoparticles have also been used for bioseparation (Park *et al* 2007). The present study shows that the magnetic core-metallic shell nanoparticles can be used for SERS applications in aqueous solution using a simple method. We show that both Ag-coated γ-Fe_2O_3 nanoparticles (γ-Fe_2O_3@AG) and Au-coated γ-Fe_2O_3 nanoparticles (γ-Fe_2O_3@Au) can be used to perform SERS at very low concentrations of analyte. By performing SERS over a wide range of temperatures, we also demonstrate the robustness of these metal-coated magnetic nanoparticles. Interestingly, a 20% Au coating on γ-Fe_2O_3 does not alter the magnetic behaviour, whereas 10% Ag coating reduces the magnetic behaviour of γ-Fe_2O_3 nanoparticles by 50%.

*Author for correspondence (cbhas@jncasr.ac.in)

2. Experimental

2.1 *Materials*

All the chemicals, $AgNO_3$ (Qualigens, 99·8%), $HAuCl_4 \cdot xH_2O$ (Loba, 49% Au), N_2H_5OH (Merck, ∼100%), $FeCl_2 \cdot 4H_2O$ (NP Chem), anhydrous $FeCl_3$ (Qualigens, 96·0%), HCl (Laboratory Rasayan, 35–38%), NaOH (Merck, 97%), HNO_3 (Laboratory Rasayan, 69–72%), 2-napthalenethiol (Aldrich, 99%), rhodamine 6G (SD fine chemicals, India, 95%) and rhodamine B (SD fine chemicals, India, 80%), were used without further purification. Millipore water was used to make the solutions.

2.2 *Synthesis*

The synthesis of γ-Fe_2O_3 nanoparticles is done following the procedures described in literature (Lyon *et al* 2004). In a typical synthetic method, 25 ml of aqueous solution containing 0·4 M Fe^{2+}, 0·8 M Fe^{3+} and 0·4 M HCl was added drop by drop to a moderately heated (∼50°C) 250 ml of aqueous 1·5 M NaOH solution under vigorous nonmagnetic stirring. A black precipitate of Fe_3O_4 was formed immediately. After 15 min of stirring the precipitates were allowed to settle down, then washed with water and magnetically separated. Again, they were washed with 0·1 M HNO_3 and centrifuged at 6000 rpm. The precipitates were then dissolved in 250 ml of 0·01 M HNO_3 and heated gently up to ∼90–100°C with constant stirring. During heating the black Fe_3O_4 turned to reddish brown due to formation of γ-Fe_2O_3. After 30 min of heating, the solution was allowed to cool to room temperature. The precipitates were centrifuged at 6000 rpm and then washed twice with water and redispersed in 500 ml water.

By using hydrazinium hydroxide as reducing agent and the seed growth method, coating of Ag or Au on γ-Fe_2O_3 was carried out. 2 ml of stock solution of γ-Fe_2O_3 (containing 0·12 mmol of Fe) was dispersed in 8 ml of water. To this 1% aqueous solution of $AgNO_3$ or 1% of $HAuCl_4$ was added to make appropriate concentration of Ag^+ or Au^{3+} in the solutions. Five sets of concentrations, 10^{-4}, 5×10^{-4}, 10^{-4}, 5×10^{-3} and 10^{-2} M each for Ag^+ and Au^{3+} were done. After 15 min, 0·2 M aqueous solution of hydrazinium hydroxide was added drop by drop with constant shaking. The final concentration of hydrazinium hydroxide had been maintained two times higher than Ag^+ or Au^{3+}. The solution turned to yellowish green for Ag and reddish brown for Au. The particles were separated by using a magnet and washed 2–3 times with distilled water and finally they were dried under vacuum at room temperature for further characterization.

2.3 *Measurements*

Transmission electron microscopy (TEM) images were recorded by using JEOL 3010 with an operating voltage of 300 keV. UV–Vis absorption measurements were done by using a Perkin–Elmer Lambda 900 UV/VIS/NIR spectrophotometer. The molar ratios of Fe to Ag or Au were determined by EDAX measurements. Magnetization measurements were performed using a VSM in physical property measurement system (PPMS) with magnetic fields up to 20 kOe at 298·15 K. The procedure is described in an earlier report (Sundaresan *et al* 2006).

SERS measurements were done by using a custom built Raman microscope as described elsewhere (Kumar and Narayana 2007). The excitation source was 632·8 nm He–Ne laser with a laser power of ∼8 mW at the sample and the typical integration time was 10 s. All the SERS experiments were done using a long working distance, high numerical aperture objective lens, which served the purpose of both, focusing the laser and collecting the Raman signals. For temperature-dependent measurements of SERS, a Linkam cryostage TMS-650 (UK) was used, as reported in Bhuvana *et al* (2007).

For solution phase experiment, a 20 μL of aqueous nanoparticle solution was mixed with 2 μL of analyte of ∼1 μM concentration. After waiting for 5 min, 10 μL of the mixture was dropped over a microscopic slide, and SERS measurements were performed using a long working distance microscope objective lens (50× SLWD objective lens, Nikon, Japan). In the case of solid films, a film was formed by drying the nanoparticles in the solution on the glass cover slip at room temperature. After the solvent evaporated, 2 μL of analyte of ∼1 μM concentration was dropped over the film followed by SERS measurements.

3. Results and discussion

Several methods are reported (Kang *et al* 1996; Lyon *et al* 2004; Mikhaylova *et al* 2004; Mandal *et al* 2005; Yusuf *et al* 2006) to synthesize γ-Fe_2O_3 superparamagnetic iron oxide nanoparticles. Amongst them, the co-precipitation of Fe^{2+} and Fe^{3+} with NaOH is one of the most simplified method to obtain polydisperse Fe_3O_4 nanoparticles, which upon further oxidation with HNO_3 yields γ-Fe_2O_3 nanoparticles (Kang *et al* 1996):

$$Fe^{2+} + 2Fe^{3+} \xrightarrow{NaOH} Fe_3O_4 \xrightarrow{HNO_3} \gamma\text{-}Fe_2O_3. \quad (1)$$

The black Fe_3O_4 nanoparticles are easily separable from the reaction mixture by using a magnet. The oxidation mechanism of Fe_3O_4 to γ-Fe_2O_3 can be confirmed by observing the change in colour from black to brown (Kang *et al* 1996). These γ-Fe_2O_3 nanoparticles are used as template for obtaining core-shell nanostructures upon coating their surface with Ag or Au. γ-Fe_2O_3 are chosen because Fe_3O_4 are unstable with respect to oxidation when compared to γ-Fe_2O_3. Hydrazinium hydroxide was used as reducing agents

for reduction of Ag^{+} or Au^{3+}. In this case, the by-products obtained are N_2 and water, thus the system is free from other contaminants, which may also give SERS signal along with the probe molecule. Another important point is that the present synthetic route does not need any surfactant. This condition further facilitates electromagnetic enhancement, which is a distance-dependent phenomena, and also helps in effective coupling of electric field to the polarizability of the molecule in SERS (Moskovits 1985; Cotton *et al* 1986). It should also be noted that Ag or Au nanoparticles obtained by using hydrazinium hydroxide without using any capping agent are unstable and aggregation occurs within 2–6 h, whereas the present nanoparticles containing magnetic core are quite stable at least for a month without using additional capping agent. The counter charge NO_3^- along with the magnetic core stabilizes the colloidal sol. Initial attempts to obtain core-shell nanostructure by using glucose, ethylene glycol and tri-sodium citrate as reducing agents yield individual Ag or Au nanoparticles, which did not serve the purpose of the present study and hence were discarded. The analytical concentration of metal to iron was varied from 1 to 50% and the content of metal in the nanostructures were determined by EDAX measurement. The reported values are the average values of 2–3 spot measurements within an accuracy of ±2%.

Figures 1(a) and (b) show the TEM images of γ-Fe_2O_3@Ag and γ-Fe_2O_3@Au nanoparticles prepared. The inset shows the corresponding images at higher magnification. The slight contrast between the core, γ-Fe_2O_3 and the shell, Ag or Au reveal the core-shell nanostructures. It is evident that there is a distribution of sizes and γ-Fe_2O_3@Ag nanoparticles appear oval, whereas γ-Fe_2O_3@Au nanoparticles appear spherical. The particles diameters are around 15 and 10 nm for γ-Fe_2O_3@Ag for (11·1% Ag + 88·9% Fe) and γ-Fe_2O_3@Ag for (21·5% Au + 81·5% Fe), respectively.

4. Surface plasmon resonance studies in metal-coated magnetic nanoparticles

The surface plasmon resonance (SPR) absorption due to the collective oscillations of free electrons in metallic nanoparticle appears in the UV-visible region, and its position depends on the shape and size of the particles as well as on the stabilizing agent and on solvent dielectric constant (Jensen *et al* 1999; Templeton *et al* 2000; Mulvaney *et al* 2003; Jensen and Schatz 2006). Figure 2(a) shows the UV-visible spectra of γ-Fe_2O_3, N_2H_4-reduced Ag and γ-Fe_2O_3@Ag (11·1% Ag + 88·9% Fe) nanoparticles. A very weak band at 350 nm was observed for γ-Fe_2O_3 nanoparticles, which may be due to the electronic excitation of oxygen lone pair. SPR bands were observed at 442 and 400 nm for Ag and γ-Fe_2O_3@Ag nanoparticles, respectively. Figure 2(b) shows the UV-visible spectra of γ-Fe_2O_3, N_2H_4-reduced Au and γ-Fe_2O_3@Au (18·5% Au + 81·5% Fe) nanoparticles. SPR bands were observed at 558 and 557 nm for Au and γ-Fe_2O_3@Au nanoparticles, respectively. Upon increasing the Ag content around γ-Fe_2O_3 nanoparticles, red shifting of the plasmon bands were observed (figure 3). However, attempts to further increase the Ag content resulted in aggregation of nanoparticles, which is a common feature of Ag coated nanoparticles (Jana 2003). Similarly, we observed red shifting of plasmon bands upon increasing the Au content, but the aggregation was lesser when compared to γ-Fe_2O_3@Ag.

5. Magnetic property of metal-coated magnetic nanoparticles

Figure 4 shows the M–H, magnetization curve for γ-Fe_2O_3, γ-Fe_2O_3@Ag and γ-Fe_2O_3@Au nanoparticles measured at 298·15 K. Like γ-Fe_2O_3, both γ-Fe_2O_3@Ag and

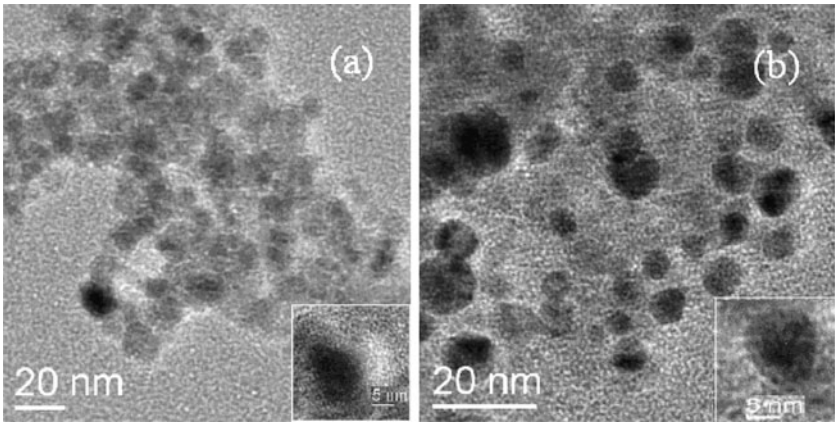

Figure 1. TEM images of (**a**) γ-Fe_2O_3@Ag for (88·9% Fe + 11·1% Ag) and (**b**) γ-Fe_2O_3@Au for (81·5% Fe + 21·5% Au) nanoparticles. The inset shows these particles at higher magnification.

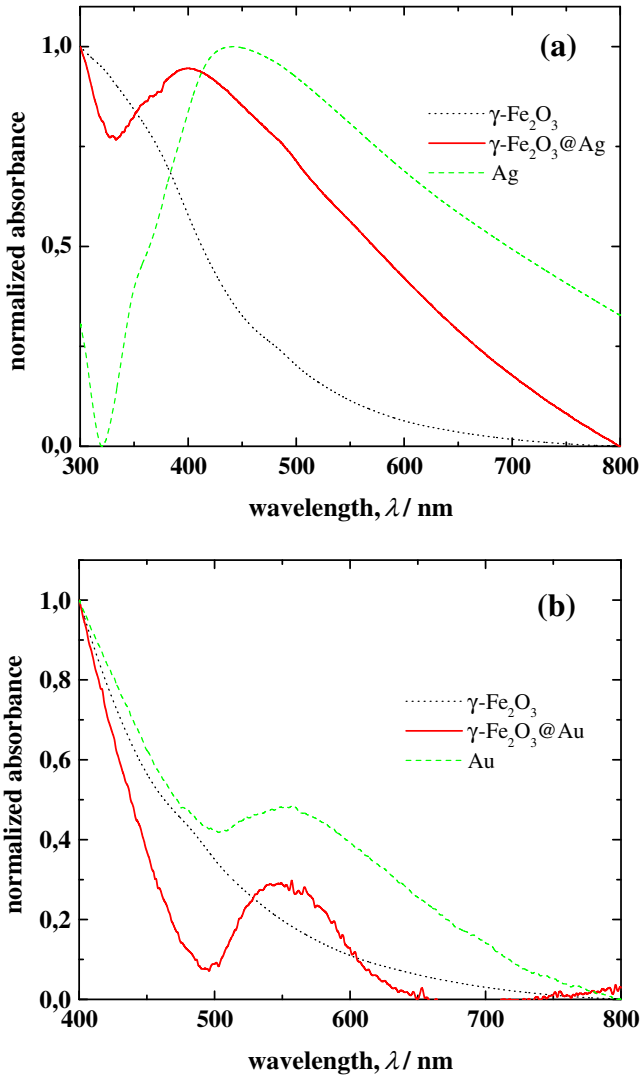

Figure 2. UV-Vis absorption spectra of γ-Fe_2O_3@Ag (solid lines in (**a**)); γ-Fe_2O_3@Au (solid lines in (**b**)); Ag sol (dashed line in (**a**)); Au sol (dashed line in (**b**)) and γ-Fe_2O_3 (dotted lines in (**a**) and (**b**)) nanoparticles, respectively.

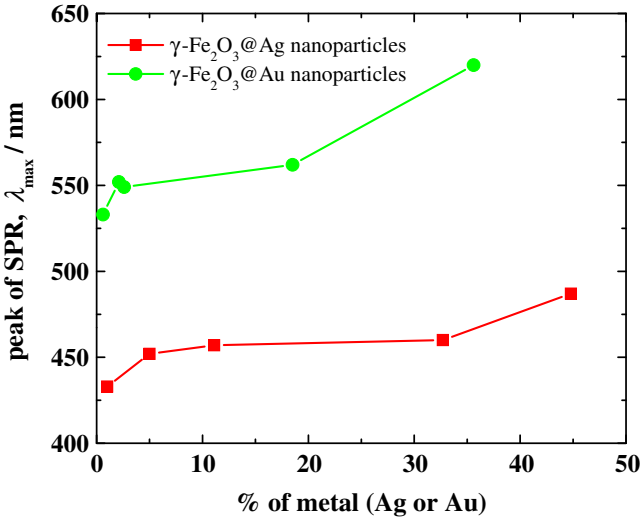

Figure 3. Variation of surface plasmon absorption against metal content in γ-Fe_2O_3@Ag and γ-Fe_2O_3@Au nanoparticles.

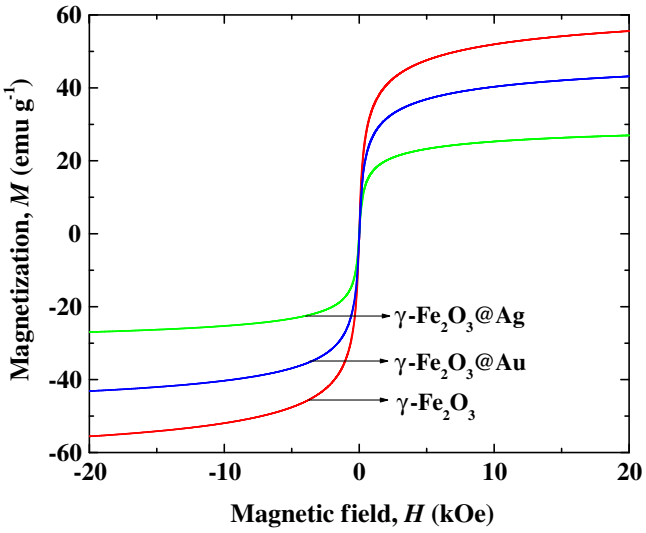

Figure 4. Plot of magnetization, M versus applied field, H at 298·15 K for γ-Fe_2O_3, γ-Fe_2O_3@Ag (88·9% Fe + 11·1% Ag) and γ-Fe_2O_3@Au (81·5% Fe + 18·5% Au) nanoparticles, respectively.

γ-Fe_2O_3@Au are super paramagnetic (SP) at room temperature. SP behaviour is observed in uncoupled ferromagnetic materials below the Curie or Neel temperature (Cullity 1972). The attribution of 'super' is due to much higher value of magnetic saturation. No hysteresis or coercivity is detectable at 298·15 K. The saturation magnetization, $M_s \approx 55{\cdot}6$ emu g^{-1} for γ-Fe_2O_3 is comparable to the reported values that vary from ~40 to 68 emu.g^{-1} (Lyon *et al* 2004; Yusuf *et al* 2006), which depends on the annealing temperature. However, this is much lower than the bulk value, ~80 emu g^{-1} (Dutta *et al* 2004). This is attributed to the greater thermal fluctuations of the smaller particles since magnetic energy is higher in larger volume. The M_s values for (88·9% Fe + 11·1% Ag) in γ-Fe_2O_3@Ag and for (81·5% Fe + 18·5% Au) in γ-Fe_2O_3@Au are observed to be ~27·0 and 43·1 emu g^{-1}, respectively. The decrease in M_s values is predominantly due to the noncontribution from Ag and Au shell towards M_s in the core shell geometry.

6. Surface enhanced Raman scattering using metal-coated magnetic nanoparticles

Although, metal-coated magnetic nanoparticles have been studied either with respect to their plasmonic (Mandal *et al* 2005) or magnetic properties (Kouassi and Irudayaraj 2006), their application in SERS study is limited (Guo *et al* 2001;

Park *et al* 2007). Since Ag and Au coated magnetic nanoparticles show strong plasmon bands in the visible wavelengths, one would expect them to exhibit SERS properties like any other core-shell nanoparticles with surface plasmon resonance. Figures 5(a) and (b) show the SERS spectra of rhodamine B (RB) and 2-napthalenethiol (NT) adsorbed on γ-Fe_2O_3@Ag and γ-Fe_2O_3@Au nanoparticles, respectively. The recorded spectra were in good agreement with the existing literature (Hildebrandt and Stockburger 1984; Alvarez *et al* 2004).

Along with the SPR, adsorption (either physisorption or chemisorption) of the analyte molecule is a pre-requirement for SERS to be observed. The orientation of the adsorbed molecule has an effect on SERS spectra. This is the case for RB where the SERS spectra show minor differences when recorded with the two core-shell nanoparticles (compare the top two spectra of figures 5(a) and (b)). This difference is in the intensity of 754 cm^{-1} band of RB adsorbed on γ-Fe_2O_3@Au and γ-Fe_2O_3@Ag. This mode corresponds to one of the substituted ring vibrations (Moskovits and DiLella 1980; Muniz *et al* 1992; Mayo *et al* 2004). In accordance with the surface selection rule (Moskovits 1982; Moskovits and Suh 1984; Campion and Kambhampati 1998) the difference in band intensity implies that RB adsorbs on γ-Fe_2O_3@Ag and γ-Fe_2O_3@Au nanoparticles with different orientations. On the other hand, NT adsorbs on the surface of γ-Fe_2O_3@Ag and γ-Fe_2O_3@Au nanoparticles with a similar orientation, and hence the spectra were found to be similar in both the cases. Also, the result in the case of RB highlights the presence of chemical enhancement, wherein the metal–molecule interactions play an important role in Raman signal enhancement.

The Raman enhancement factor in solution phase for NT adsorbed on to γ-Fe_2O_3@Ag and γ-Fe_2O_3@Au nanoparticles was calculated and found to be 10^6 and 10^5, respectively. The details of the calculation can be found elsewhere (Kumar *et al* 2007). These values are on par with the enhancement factors of conventional Ag and Au nanoparticles (Aroca *et al* 2005). The enhancement factor could be further increased by using aggregating agents like NaCl or LiCl, due to the chloride ion effect (Otto *et al* 2003). We have observed that the SERS signal is enhanced by 50 times when 0·5 M NaCl is added. This phenomenon is analogous to the effect observed by Hofmeister who originally observed the effect of added electrolyte on protein solubilities (Hofmeister 1887). The added anion enhances the adsorption of the analyte on the nanoparticles, resulting in greater Raman scattering.

Rhodamine 6G (R6G) adsorbed nanoparticles were dried on glass slide to form a film. Figure 6(a) shows the SERS spectra of R6G adsorbed to γ-Fe_2O_3@Ag in solution as well as on film. It is observed that the film phase spectrum is enhanced by a factor of 10 compared to the solution phase. This difference could be ascribed to variation in surface plasmon resonance of the nanoparticles in solution and film phase (Moskovits 1985). Since these nanoparticles are magnetic in nature, they are aggregated when an external magnetic field is applied. This strategy facilitates intense optical field for molecules that reside at the junction of two particles, which further leads to improvement in SERS sensitivity. It has been observed that the Raman signal of R6G adsorbed

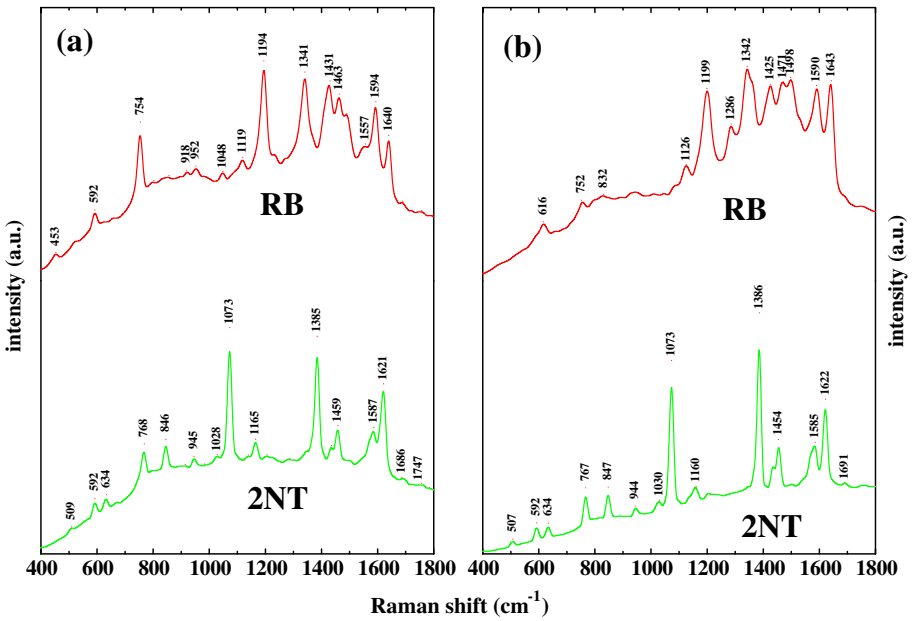

Figure 5. SERS spectra of rhodamine B (RB), top and 2-napthalenethiol (2NT), bottom adsorbed on (**a**) γ-Fe_2O_3@Ag and (**b**) γ-Fe_2O_3@Au nanoparticles and recorded at room temperature (22°C). The excitation wavelength used was 632·8 nm.

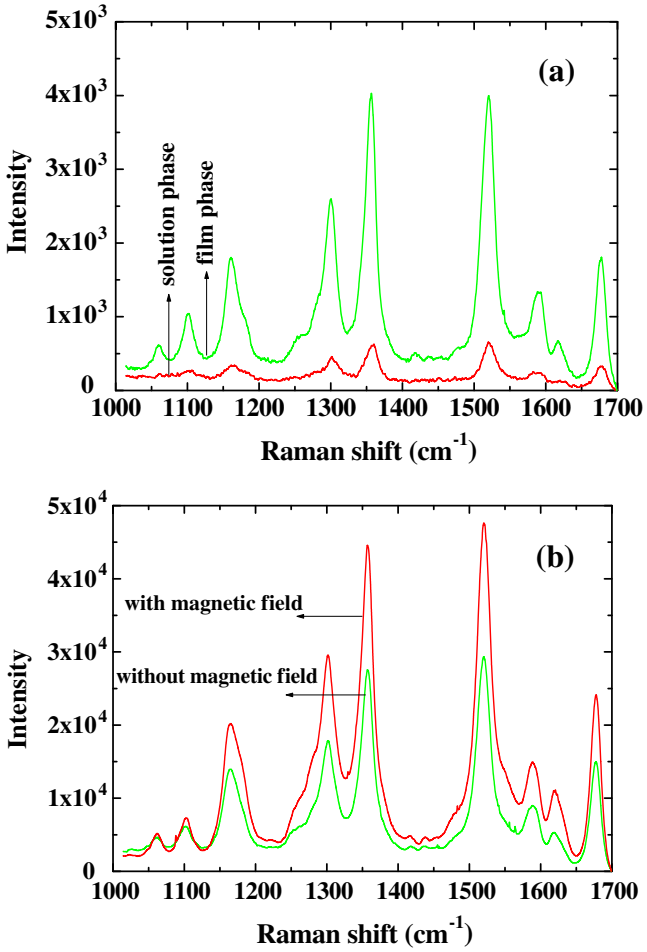

Figure 6. SERS spectra of (**a**) rhodamine 6G adsorbed to γ-Fe_2O_3@Ag in solution and in film phase and (**b**) rhodamine 6G adsorbed to γ-Fe_2O_3@Au in absence and presence of magnetic field.

on γ-Fe_2O_3@Au nanoparticles is enhanced by a factor of 2 (figure 6(b)).

7. Temperature dependent SERS using γ-Fe_2O_3@Ag nanoparticles

Along with pressure, temperature is one of the most important thermodynamic parameter to test the robustness of materials. Raman scattering has been a well-established tool to study temperature and pressure-dependant phenomenon (Long 1977; Manfait and Nabiev 1996). Of late, due to advancement in optical and cryogenic instrumentation, temperature-dependant SERS has evolved as a new technique to test fundamental aspects (Maher *et al* 2006) and applications (Bhuvana *et al* 2007) of nanoparticle films. In order to test the robustness of metal-coated magnetic nanoparticle film, we have performed temperature-dependent SERS on γ-Fe_2O_3@Ag nanoparticles drop coated over a microscope cover slip. Figure 7 shows the SERS of NT adsorbed

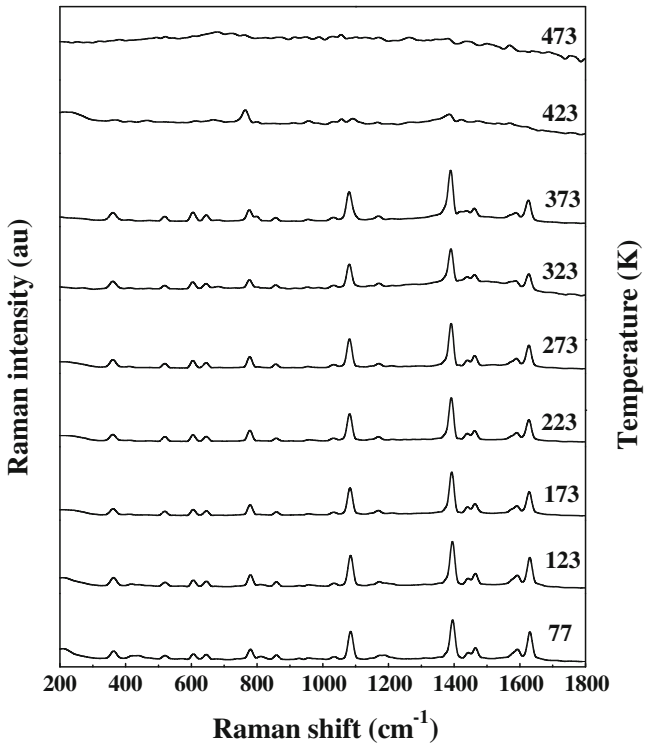

Figure 7. Temperature dependence of 2-napthalenethiol on γ-Fe_2O_3@Ag in the range of 77 K to 473 K. The spectra have been vertically shifted for clarity.

to γ-Fe_2O_3@Ag nanoparticles in the temperature range of 77–473 K. We observed that the SERS spectra are consistently same over a wide range of temperature ($323 \geq T(\mathrm{K}) \geq 77$), which confirms the robustness of γ-Fe_2O_3@Ag. Beyond 323 K, the SERS spectra change due to the change in the orientation of adsorbed molecules. At 473 K, the thermal desorption of NT occurs thus resulting in the disappearance of the SERS spectra (Kolega and Schlenoff 1998; Kim *et al* 2002). This is in agreement with the fact that the adsorption of analyte molecules on colloidal particles as one of the prerequisite for obtaining considerable enhancement in the Raman scattering signal. Moreover, the enthalpy of adsorption, $\Delta H_{\mathrm{ads}} \approx RT$ suggests a value of $\sim$4 kJ mol^{-1} that NT is physisorbed on γ-Fe_2O_3@Ag (for chemisorptions, the condition is $50 < \Delta H_{ads}/$ kJ mol^{-1} < 800). This shows the sensitivity of the technique to detect the change in adsorption properties of molecules, and proves the efficiency of the metal-coated magnetic nanoparticle film as a SERS substrate.

8. Magnetic field assisted manoeuvring of γ-Fe_2O_3@Au nanoparticle aggregates and their SERS effect

The physical control, assembly and manoeuvrability of submicron matter have various applications in different aspects

of science and technology (Terfort *et al* 1997; Whitesides and Grzybowski 2002). Nanoparticles are one such paradigm of sub-micron matter with a variety of interesting physical properties. The surface-enhanced Raman scattering and magnetism are two of the many attributes of nanoparticles, which have been studied for γ-Fe_2O_3@Au nanoparticles under an external magnetic field. A 20 μL drop of γ-Fe_2O_3@Au was deposited on a glass cover slip and placed underneath a 10× objective lens of the Raman microscope. Toward one end of the deposited solution of nanoparticle, a bar magnet of strength 0·5 T was placed at a distance of 1 cm and locked. Care was taken to avoid any contact between the deposited solution and the magnet. As soon as the magnetic field was applied, the nanoparticles moved towards the magnet and formed microscopically visible aggregates (∼30 μm wide) at the edge of the solution. The rate of aggregation and the width of the aggregate depend on the distance between the magnet and the solution. Figure 8 shows the aligned aggregates for three different directions (45°, 0° and −45°) of magnetic field. The white arrows in figure 8 represent the direction of the magnetic field. As can be observed in the figure, towards the end, where the magnet was placed, a thick dark aggregate formed with fibrils. These fibrils are elongated clusters of nanoparticles. The direction of the fibrils shows that aggregate tends to align along the magnetic flux lines. In order to flip the direction of aligned aggregate, we just had to change the direction of the magnet, and the response of the aggregate was instantaneous. The fibrils, which are compacted in the presence of magnetic field, tend to exhibit Brownian motion in the absence of the field, and again move towards the aggregate as soon as the magnet was moved in close proximity. To understand this alignment behaviour, we can consider the whole aggregate to comprise of numerous clusters of magnetic nanoparticles. The self assembly happens at both the ensemble levels (the whole aggregate) and at the individual particle level. At the ensemble level, the magnetization vector of each cluster in the aggregate couples to an effective field, H_{eff}, which is superposition of two components. The first one would be the dominant, applied magnetic field, and the other would be the weak, local field created by the clusters of neighbouring nanoparticles. If the elongated cluster in the aggregate can be approximated to an ellipsoidal particle that has a shape-induced uniaxial anisotropy, with the easy axis along its length, then the magnetostatic energy, E, of the cluster is given by (Cullity 1972; Sahoo *et al* 2004):

$$E = 1/2\ M^2 V N_{\text{L}} + 1/2\ M^2 V\ (N_{\text{S}} - N_{\text{L}}) \sin^2 q - H_{\text{eff}}\, MV\ \cos\phi, \tag{2}$$

where V is volume of the aggregate, M the modulus of the magnetization vector, N_{L} and N_{S} are demagnetization factors along long and short axes, respectively; θ the angle between the long axes and magnetization vector, and ϕ the angle between the effective field and long axis. The magnetostatic energy would be minimal when the last term in (2) has the greatest value. This can be achieved when the direction of the effective field and the long axis are the same, i.e. when $\phi = 0$. This explains the tendency of the aggregate to align along the field direction.

Next, we discuss the formation of a thin film of γ-Fe_2O_3@Au on a glass cover slip. A 20 μL drop of γ-Fe_2O_3@Au was placed on a cleaned glass cover slip, which was 2 cm away from a 0·5 T bar magnet. The solution was left as it was for 2 h without any movement. By then, all the solvent had evaporated, and a film of γ-Fe_2O_3@Au was formed. Figure 9(a) shows a white light illuminated, transmission mode and an optical image of the film formed. It was evident from the image that the film had two distinct regions: an opaque, cracked region; and a translucent, aligned nanoparticle, strip region. These regions were continuous along the plane of the cover slip with distinct colour contrast. The interface region between these phases had a colour gradient, which varied from dark brown, to red, and finally merged into the yellow background. We observed same kind of assembly of γ-Fe_2O_3@Au on a silicon surface, which was imaged using a field emission scanning electron microscope (FESEM) as shown in figures 10(b) and (c). The cracked film (figure 9(a)) resembled cracks formed on dry soil, and comprised of smooth, distinct, rectangular and square shaped islands, whose boundaries were well defined. A higher resolution FESEM image of an island showed that the cracked film was a compaction of nanoparticles. The main reason behind the crack formation would be the drying-mediated aggregation of nanoparticles (Rabani *et al* 2003) in the presence of a magnetic field, where heterogeneous

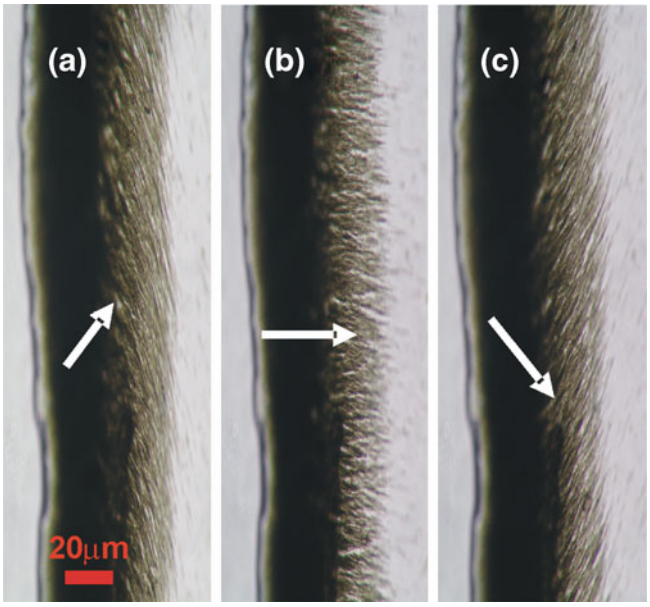

Figure 8. Magnetic field induced alignment of Fe_2O_3@Au aggregates along three different angles: (**a**) 45°, (**b**) 0° and (**c**) −45°. The white arrows indicate the direction of the magnetic field.

limits of evaporation dynamics (Rabani *et al* 2003) and domain instabilities (Seul and Andelman 1995) play a major role. Figure 9(c) shows an FESEM image of the film formed ~10 cm away from the magnet. Long strips of γ-Fe_2O_3@Au were observed, whose length varied from 100 nm to 10 μm. A high resolution FESEM image revealed that these strips were aligned aggregates of nanoparticles, with a rough surface morphology at the nano-scale. These kinds of strip formation in the presence of magnetic field have been reported earlier for various magnetic nanomaterials (Gelbart *et al* 1999; Tanase *et al* 2001, 2005; Sahoo *et al* 2004). It is to be noted that in the absence of a magnetic field, neither a cracked film nor the formation of strips were observed when a γ-Fe_2O_3@Au drop was evaporated.

Figure 10(a) shows the magnetization curve recorded for a cracked film (black curve), and a film containing the aligned strips of nanoparticles (gray curve). Although both these regions of nanoparticles exhibited super paramagnetic behaviour, the magnetic saturation value of the cracked film was higher than the film with aligned magnetic nanoparticles. This is because, the cracked film is a compact structure formed due to the field-induced aggregation of nanoparticles, and hence the density of the magnetic spins would be greater. Whereas, in the case of films with strips of nanoparticles, the particle density was lesser than the surface of a cracked film, which results in a lower magnetic saturation. Having observed a difference in the roughness of the two phases of a γ-Fe_2O_3@Au film, we tested them for SERS behaviour. Figure 10(b) shows the SERS spectra of naphthalenethiol (NT) adsorbed on a cracked film (black curve), and on strips of nanoparticles (gray curve). We observed a large Raman

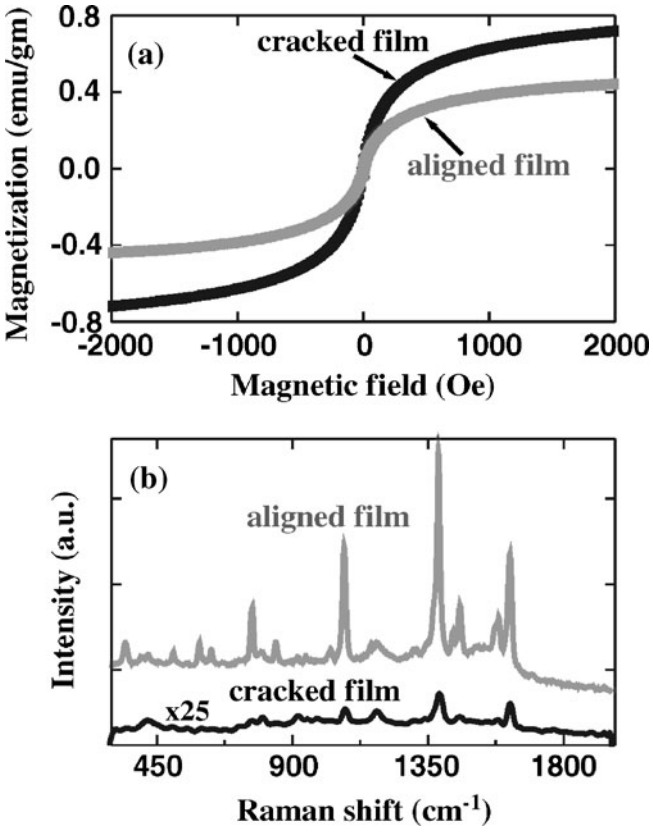

Figure 10. (**a**) Magnetization plots of cracked Fe_2O_3@Au film and aligned Fe_2O_3@Au film and (**b**) SERS spectra of napthalenethiol adsorbed to cracked and aligned Fe_2O_3@Au film, laser excitation was 632·81 nm and signal accumulation time was 10 s.

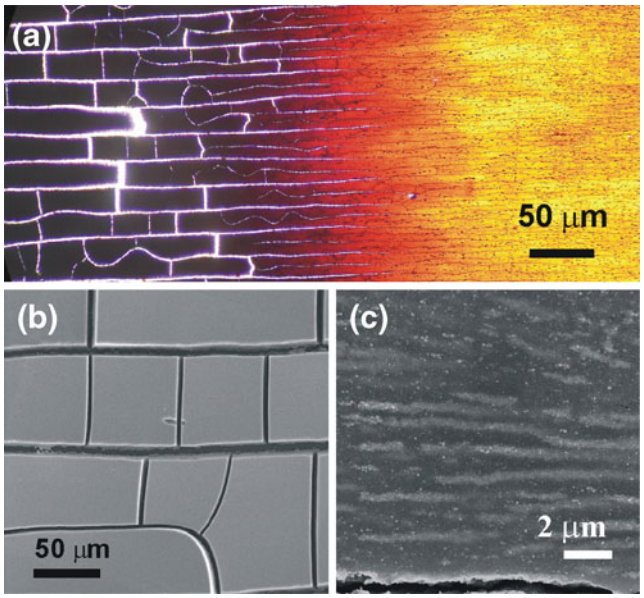

Figure 9. Magnetic field assembled Fe_2O_3@Au films. (**a**) Optical image captured in transmission mode, (**b**) FE–SEM image of cracked film and (**c**) FE–SEM image of aligned nanoparticles.

signal enhancement ability of the nanoparticle strips when compared to the cracked film. The ratio of enhancement factors (Moskovits 1985) for the 1360 cm^{-1} band of NT adsorbed to the two phases was of the order of 10^4. This large difference in SERS behaviour is due to the difference in the surface roughness of the two regions of the film. Since the morphology of cracked film was observed to be smooth, one would expect the localized surface plasmon to be absent (Moskovits 1985). Whereas, in case of the rough strips of nanoparticles, there would be localized surface plasmons (Willets and Duyne 2007) at various 'hot spots', which further facilitate huge optical fields that couple to the polarizability of the molecule. This leads to an enhanced Raman signal. Also, one would expect the plasmonic properties of the two phases in the film to be different from each other, which would account for the difference in the enhancement factor.

9. Conclusions

A new synthetic strategy has been devised to prepare water dispersible, surfactantless, Ag and Au coated magnetic

nanoparticles for SERS applications. These paramagnetic nanoparticles have been used for SERS detection of molecules, and have been found to be on par with the conventional Ag and Au nanoparticles. We have also shown that γ-Fe_2O_3@Au nanomaterial can be magnetically manipulated with a high degree of control. By forming a film of γ-Fe_2O_3@Au, we have shown that the hybrid nature of the zero-dimensional nanoparticles can be extrapolated to one-dimensional nanoparticle strip, and two-dimensional cracked surfaces. Apart from exhibiting excellent surface plasmon resonance, these nanoparticles are superparamagnetic at room temperature, which opens new avenues for detection methodologies. Since these nanoparticles can be dispersed in aqueous solution, they are ideal for biological application without any further modification. Work is in progress towards functionalizing metal-coated magnetic nanoparticles with selected proteins that are covalently linked to Raman markers. This composite can be further introduced into a living cell, and tracked by both, SERS and magnetic field.

Acknowledgements

The authors thank C Madhu, P Mandal and Dr A Sundaresan of CPMU, JNCASR, for the magnetic measurements. The DST unit on Nanoscience is acknowledged for the FESEM facility. Ms R Selvi is thanked for FESEM imaging. (CN) would like to thank POCE program of CPMU, JNCASR, for providing the opportunity to N Rangarajan to work in LSL.

References

Alvarez P R A, Dos S Jr and Aroca R F 2004 *The Analyst* **129** 1251
Aroca R F, Alvarez P R A, Pieczonka N, Sanchez C S and Garcia R J V 2005 *Adv. Colloid Interface Sci.* **116** 45
Aslan K, Wu M, Lakowicz J R and Geddes C D 2007 *J. Am. Chem. Soc.* **129** 1524
Baker G A and Moore D S 2005 *Anal. Bioanal. Chem.* **382** 1751
Barnes W L, Dereux A and Ebbesen T W 2003 *Nature* **424** 824
Bhuvana T, Kumar G V P, Kulkarni G U and Narayana C 2007 *J. Phys. Chem.* **C111** 6700
Campion A and Kambhampati P 1998 *Chem. Soc. Rev.* **27** 241
Cotton T M, Uphaus R A and Mobius D 1986 *J. Phys. Chem.* **90** 6071
Cullity B D 1972 *Introduction to magnetic materials* (Reading: Addison-Wesley)
Dieringer J A, McFarland A D, Shah N C, Stuart D A, Whitney A V, Yonzon C R, Young M A, Zhang X and Van Duyne R P 2006 *Faraday Discuss.* **132** 9
Dutta P, Manivannan A, Seehra M S, Shah N and Huffman G P 2004 *Phys. Rev.* **B70** 174428
Freeman R G, Hommer M B, Garbar K C, Jackson M A and Natan M J 1996 *J. Phys. Chem.* **100** 718
Gelbart W M, Sear R P, Heath J R and Chaney S 1999 *Faraday Discuss.* **112** 299
Genet C and Ebbesen T W 2007 *Nature* **445** 39
Guo L, Huang Q, Li X Y and Yang S 2001 *Phys. Chem. Chem. Phys.* **3** 1661
Hildebrandt P and Stockburger M 1984 *J. Phys. Chem.* **88** 5935
Hofmeister F 1887 *Arch. Exp. Pathol. Pharmacol.* **29** 1
Hutter E and Fendler J H 2004 *Adv. Mater.* **16** 1685
Jana N R 2003 *The Analyst* **128** 954
Jensen T R and Schatz G C 2006 *J. Phys. Chem.* **A110** 5973
Jensen T R, Schatz G C and Van Duyne R P 1999 *J. Phys. Chem.* **B103** 2394
Jin R, Charles C Y, Hao E, Metraux G S, Schatz G C and Mirkin C A 2003 *Nature* **425** 487
Kang Y S, Risbud S, Rabolt J F and Stroeve P 1996 *Chem. Mater.* **8** 2209
Kim C, Sim J H, Yan X M and White J M 2002 *Langmuir* **18** 3159
Kneipp K, Kneipp H, Itzkan I, Dasari R R and Feld M S 1999 *Chem. Rev.* **99** 2957
Kneipp K, Moskovits M and Kneipp H 2006 *Surface-enhanced Raman scattering, physics and applications* (Berlin, Heidelberg: Springer-Verlag)
Kolega R R and Schlenoff J B 1998 *Langmuir* **14** 5469
Kouassi G K and Irudayaraj J 2006 *Anal. Chem.* **78** 3234
Kumar G V P and Narayana C 2007 *Curr. Sci.* **93** 778
Kumar G V P, Shruthi S, Vibha B, Reddy B A A, Kundu T K and Narayana C 2007 *J. Phys. Chem.* **C111** 4388
Long D A 1977 *Raman spectroscopy* (New York: McGraw Hill)
Lyon J L, Fleming D A, Stone M B, Schiffer P and Willians M E 2004 *Nano Lett.* **4** 719
Maher R C, Cohen L F, Gallop J C, LeRu E C and Etchegoin P G 2006 *J. Phys. Chem.* **B110** 6797
Mandal M, Kundu S, Ghosh S K, Panigrahi S, Sau T K, Yusuf S M and Pal T 2005 *J. Colloid Interface Sci.* **286** 187
Manfait M and Nabiev I 1996 *Raman microscopy* (London: Academic Press)
Mayo D W, Miller F A and Hannah R W 2004 *Course notes on the interpretation of infrared and Raman spectra* (New Jersey: Wiley)
Mikhaylova M, Kim D K, Bobrysheva N, Osmolowsky M, Semenov V, Tsakalakos T and Muhammed M 2004 *Langmuir* **20** 2472
Moskovits M 1982 *J. Chem. Phys.* **77** 4408
Moskovits M 1985 *Rev. Mod. Phys.* **57** 783
Moskovits M and DiLella D P 1980 *J. Chem. Phys.* **73** 6068
Moskovits M and Suh J S 1984 *J. Phys. Chem.* **88** 5526
Mulvaney S P, Musick M D, Keating C D and Natan M J 2003 *Langmuir* **19** 4784
Muniz M M, Neto N and Sbrana G 1992 *J. Mol. Struct.* **267** 281
Otto A, Bruckbauer A and Chen Y X 2003 *J. Mol. Struct.* **661–662** 501
Park H Y, Schadt M J, Wang L, Lim I I S, Njoki P N, Kim S H, Jang M Y, Luo J and Zhang C J 2007 *Langmuir* **23** 9050
Pramod P, Joseph S T S and Thomas K G 2007 *J. Am. Chem. Soc.* **129** 6712
Previte M J R, Aslan K, Zhang Y and Geddes C D 2007 *J. Phys. Chem.* **C111** 6051
Rabani E, Reichman D R, Geissler P L and Brus L E 2003 *Nature* **426** 271
Sahoo Y, Cheon M, Wang S, Luo H, Furlani E P and Prasad P N 2004 *J. Phys. Chem.* **B108** 3380
Seul M and Andelman D 1995 *Science* **267** 476
Shibu J S T, Ipe B I, Pramod P and Thomas K G 2006 *J. Phys. Chem.* **B110** 150

Sundaresan A, Bhargavi R, Rangarajan N, Siddesh U and Rao C N R 2006 *Phys. Rev.* **B74** 161306
Tanase M, Bauer L A, Hultgren A, Silevitch D M, Sun L, Reich D H, Searson P C and Meyer G J 2001 *Nano Lett.* **1** 155
Tanase M, Felton E J, Gray D S, Hultgren A, Chen C S and Reich D H 2005 *Lab. Chip Miniaturization Chem. Biol.* **5** 598
Templeton A C, Pietron J J, Murray R W and Mulvaney P 2000 *J. Phys. Chem.* **B104** 564
Terfort A, Bowden N and Whitesides G M 1997 *Nature* **386** 162
Thomas K G, Barazzouk S, Ipe B I, Joseph S T S and Kamat P V 2004 *J. Phys. Chem.* **B108** 13066
Vlaminck I D, Dorpe P V, Lagae L and Borghs G 2007 *Nano Lett.* **7** 703
Whitesides G M and Grzybowski B 2002 *Science* **295** 2418
Willets K A and Duyne R P V 2007 *Ann. Rev. Phys. Chem.* **58** 267
Wurtz G A, Evans P R, Hendren W, Atkinson R, Dickson W, Polland R J, Harrison W, Bower C and Zayats A V 2007 *Nano Lett.* **7** 1297
Xu Z, Hou Y and Sun S 2007 *J. Am. Chem. Soc.* **129** 8698
Yusuf S M, De Teresa J M, Mukadam M D, Kohlbrecher J, Ibarra M R, Arbiol J, Sharma P and Kulshreshtha S K 2006 *Phys. Rev.* **B74** 224428
Zhang W, Cui X D, Yeo B S, Chmid T, Hafner C and Zenobi R 2007a *Nano Lett.* **7** 1401
Zhang J, Fu Y and Lakowicz J R 2007b *J. Phys. Chem.* **C111** 50